

River-plume sedimentation and $^{210}\text{Pb}/^7\text{Be}$ seabed delivery on the Mississippi River delta front

Gregory Keller^{1,2} · Samuel J. Bentley^{1,2} · Ioannis Y. Georgiou⁴ · Jillian Maloney⁵ · Michael D. Miner⁶ · Kehui Xu^{1,3}

Received: 27 September 2016 / Accepted: 10 October 2016
© Springer-Verlag Berlin Heidelberg 2016

Abstract To constrain the timing and processes of sediment delivery and submarine mass-wasting events spanning the last few decades on the Mississippi River delta front, multi-cores and gravity cores (0.5 and <3 m length respectively) were collected seaward of the Mississippi River Southwest Pass in 25–75 m water depth in 2014. The cores were analyzed for radionuclide activity (^7Be , ^{210}Pb , ^{137}Cs), grain size, bulk density, and fabric (X-radiography). Core sediments are faintly bedded, sparsely bioturbated, and composed mostly of clay and fine silt. Short-term sedimentation rates (from ^7Be) are 0.25–1.5 mm/day during river flooding, while longer-term accumulation rates (from ^{210}Pb) are 1.3–7.9 cm/year. In most cores, ^{210}Pb activity displays undulatory profiles with overall declining activity versus depth. Undulations are not associated with grain size variations, and are interpreted to represent variations in oceanic ^{210}Pb scavenging by river-plume sediments. The ^{210}Pb profile of one gravity core from a mudflow gully displays uniform basal excess activity over a zone of low

and uniform bulk density, interpreted to be a mass-failure event that occurred 9–18 years before core collection. Spatial trends in sediment deposition (from ^7Be) and accumulation (from ^{210}Pb) indicate that proximity to the river mouth has stronger influence than local facies (mudflow gully, depositional lobe, prodelta) over the timeframe and seabed depth represented by the cores (<40 years, <3 m length). This may be explained by rapid proximal sediment deposition from river plumes coupled with infrequent tropical cyclone activity near the delta in the last 7 years (2006–2013), and by the location of most sediment failure surfaces (from mass flows indicated by parallel geophysical studies) deeper than the core-sampling depths of the present study.

Introduction

Muddy clinothems on continental shelves are commonly built with sediment delivered from a fluvial source, shaped by cross-shelf gradients in sediment accumulation (e.g., Slingerland et al. 2008). The morphology of such deltaic deposits is further influenced by dispersal processes including but not limited to waves, tides, and fluvial flows (Wright and Coleman 1973; Galloway 1975; Walsh and Nittrouer 2009). The Mississippi River delta has long been considered a river-dominated end-member of deltaic morphology (Wright and Coleman 1973; Galloway 1975; Walsh and Nittrouer 2009), wherein major morphological features are produced by interacting river flows (delivering abundant sediment) and subsequent mass failures that remobilize and redistribute sediments (Coleman et al. 1980). These phenomena are characteristic of the Mississippi River delta front (MRDF; Coleman et al. 1980), which is morphologically equivalent to the submarine foreset beds of the prograding Mississippi River delta and clinothem (Wright and Coleman 1973).

✉ Samuel J. Bentley
sjb@lsu.edu

¹ Coastal Studies Institute, Louisiana State University, Baton Rouge, LA 70803, USA

² Department of Geology and Geophysics, Louisiana State University, Baton Rouge, LA 70803, USA

³ Department of Oceanography and Coastal Sciences, Louisiana State University, Baton Rouge, LA 70803, USA

⁴ Department of Earth and Environmental Sciences, University of New Orleans, New Orleans, LA 70148, USA

⁵ Department of Geological Sciences, San Diego State University, San Diego, CA 92182, USA

⁶ U.S. Department of the Interior, Bureau of Ocean Energy Management, New Orleans, LA 70123, USA

Submarine mass failures are associated with many deltas worldwide that are considered “river dominated”, or characterized by rapid proximal sediment accumulation (Prior and Coleman 1982; Walsh and Nittrouer 2009). Specific examples include the Niger (Sultan et al. 2007), Fraser (Hart et al. 1998), and Huanghe (Prior et al. 1989). Because pipelines, communication lines, navigation aids and channels, and other infrastructure are commonly located in such areas, understanding specific forces that control seabed dynamics in such deltaic settings has broad significance.

The first major insights into submarine mass movements of the MRDF were primarily derived from the comparison of bathymetric surveys (Shepard 1955), and early applications of sidescan sonar (Coleman et al. 1980). Coleman et al. (1980) and Prior and Suhayda (1979) described the motion of sediments in mudflow lobes, gullies, and other similar landforms as either slow, steady creeps or rapid movements that pulse over time, with downslope movement rates from hundreds of meters to up to 2 km per year. These insights were gained primarily via repeat geophysical surveys, with little sediment geochronology. More recent work has evaluated regional dispersal patterns using radioisotope geochronology (Corbett et al. 2006; Young 2014); in these studies, radiochemical tracers were used to study sedimentation rates and the annual input of sediment to the continental shelf. These radiochemical studies have focused mostly on regional-scale phenomena on the Mississippi delta continental shelf. However, interplays between plume sedimentation and mass-wasting processes on the MRDF remain poorly documented, except following extreme events such as Hurricane Katrina in 2005 (Goni et al. 2007). Thus, there is a sizeable knowledge gap in our understanding of this highly dynamic depositional setting.

Concerns regarding seafloor stability of the MRDF, associated mass wasting, and risk to petroleum production infrastructure focused interest on MRDF mass failures decades ago (e.g., Bea 1971), and have been renewed since hurricanes Ivan (in 2004) and Katrina (Guidroz 2009; Kaiser et al. 2009). The present study applies radioisotope geochronological proxies (^{210}Pb , ^{137}Cs , and ^7Be) and other geological core analyses to evaluate sediment depositional and dispersal processes (including fluvial supply and mass failures) across the MRDF over timescales of seasons to decades and sub-seabed depths up to 3 m. The primary objective was to evaluate the relative role of sediment delivery from river plumes with respect to subsequent remobilization by mudflows on creating the sedimentary strata of the MRDF. This work differs from previous studies of mudflows on the MRDF, which have mostly used geophysical and geotechnical approaches to evaluate catastrophic failures associated with major hurricanes (e.g., Prior et al. 1989; Hooper and Suhayda 2005). Numerous studies of sedimentary processes have been conducted on the shelf adjacent to the Mississippi delta using ^{210}Pb and ^7Be

geochronology, but most were based on cores distributed widely over areas $>1,000\text{ km}^2$, whereas the present study focuses on detailed perspectives within a region $<100\text{ km}^2$ near Southwest Pass where plume sedimentation and mudflows are thought to be most closely connected (Coleman et al. 1980). This work forms part of a larger study of MRDF mass-wasting processes and products (Fig. 1b, c), focused on developing a more complete understanding of the rates and spatiotemporal distribution and scales of mass wasting on the MRDF (discussed in Bentley et al. 2015).

Background

Study area

The study area is the continental shelf proximal to the Southwest (SW) Pass distributary of the Mississippi River (MR), spanning water depths from 25 to 75 m (Fig. 1). SW Pass is the largest of three major distributary outlets of the modern Balize or bird-foot delta of the MR (Allison et al. 2012). The MR delivers approximately 2×10^8 metric tons of suspended sediment to the northern Gulf of Mexico each year (Meade 1996). For water years (1st October–30th September) 2008–2010, SW Pass discharged $\sim 2\times 10^7$ metric tons of sediment per year, with the remainder of sediment exiting the river from other outlets (Allison et al. 2012). Much of the sediment is initially retained near the distributaries (within $\sim 30\text{ km}$; Corbett et al. 2004; Xu et al. 2011), before being redistributed by tropical cyclones and other weather systems (Wright and Nittrouer 1995; Bentley 2002; Walsh et al. 2006). Wright and Nittrouer (1995) note that fair-weather conditions on the MRDF do not retard the settling of sediment, and cannot resuspend it, making the MRDF prone to proximal sediment accumulation (sensu Walsh and Nittrouer 2009). Subsequent sediment remobilization can be achieved by less frequent storm resuspension and mass wasting, which is also associated with storm waves. Mass wasting constitutes the dominant seabed signature of geomorphic processes (Coleman et al. 1980; Fig. 2). Mass-failure events pose a significant hazard to the vast array of oil and gas drilling platforms and pipelines in the area (Sterling and Strohbeck 1973; Guidroz 2009; Kaiser et al. 2009).

Causes of mass failures

Mass failures develop where and when the downslope force of gravity acting on a mass of sediment exceeds resisting forces (Lee et al. 2009). Mass failures on the MRDF are facilitated by the low strength of seafloor sediments. Coleman et al. (1980) proposed a four-part model for mass failures: (1) rapid sedimentation that (2) prohibits dewatering followed by (3) charging with biogenic gas, culminating in (4) movements triggered

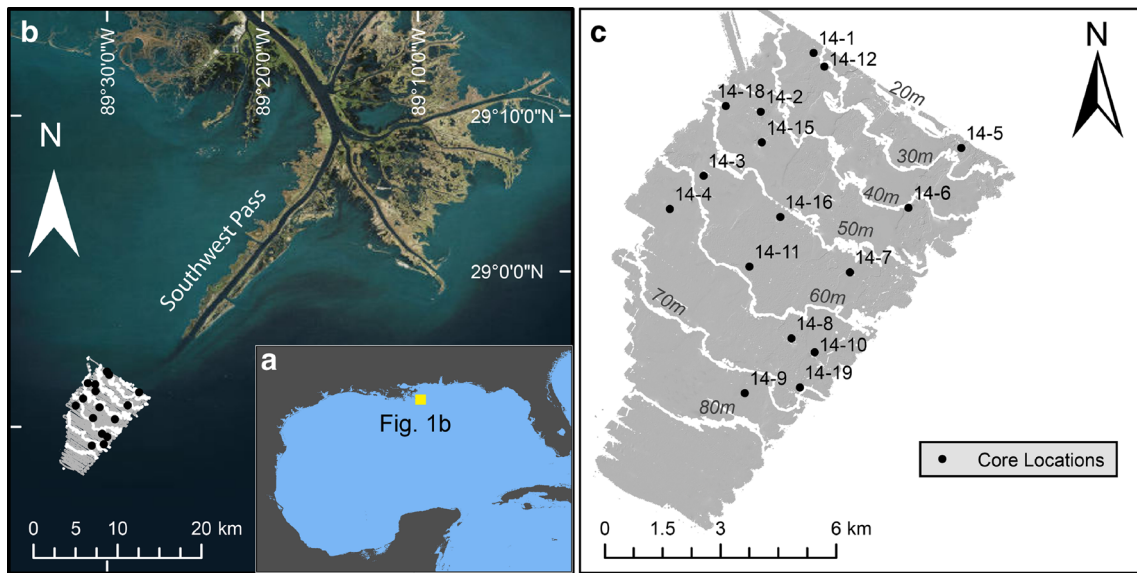


Fig. 1 Map of study area, with location **a** in the Gulf of Mexico and **b** near Southwest Pass. **c** Coring locations (dots, with codes) on contoured bathymetry from Walsh et al. (2006), with contours as wide white lines, and contour labels (meters below sea level) in gray italics. Some locations

include both a short core and a gravity core. In the text, the gravity cores are identified by a “g” following the core location code. Contour intervals are 10 m. Background imagery for **a** is open source “World Imagery” from ESRI

by shear stresses associated with long-period storm waves. The formation of “weak plastic sediments” is the result of rapid sedimentation (25 cm in a month, Coleman et al. 1980; 8 cm from the 2011 flood layer on the Atchafalaya shelf, Young 2014) of low-permeability silts and clays that inhibit pore-water flow. Gas-charged sediments have been confirmed across the Louisiana shelf by J. Obelcz et al. (unpubl. data; SW Pass area) and Denomme and Bentley (2013; southwest coast of Louisiana, near Atchafalaya River outflow). These unstable sediments can then be weakened to the point of failure by cyclic loading associated with storm waves. Large waves (Coleman et al. 1980) produced by major hurricanes crossing the Mississippi River delta are known to be major

controls on the development of large seabed failures (Guidroz 2009), but more recent work (Denomme and Bentley 2013) also demonstrates that much smaller waves from ~weekly winter cold fronts are also capable of initiating smaller flows closer to shore in waters <10 m deep. Assessing the range of conditions over which such failures can occur, and their geological record, is one goal of this study.

Sediment transport processes and seabed morphology

Figure 2 illustrates major elements of MRDF seabed morphology, using the terminology of Coleman et al. (1980), bathymetry from Walsh et al. (2006), and subsurface structure

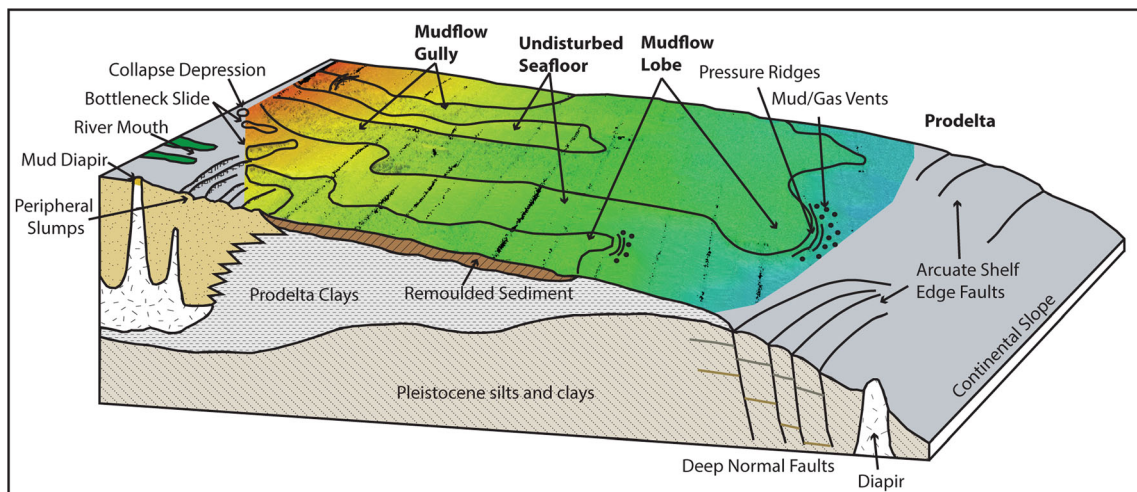


Fig. 2 Seafloor diagram illustrating morphological facies. Adapted from Coleman et al. (1980) by J. Maloney et al. (unpubl. data) using multi-beam bathymetry data from Walsh et al. (2006). Outlined mudflow

gullies cut into undisturbed seafloor and convey sediment downslope to depositional lobes, which may stack and coalesce. The range of depth is 20–80 m, with warmer colors corresponding to shallower depths

interpreted from Coleman et al. (1980) and J. Obelcz et al. (pers. comm.). Mudflow gullies are prevalent from interdistributary bays down through the intermediate delta front (120 m depth). Gullies can incise up to 20 m into the undisturbed seafloor, and extend laterally up to 10 km across the shelf, joining with other channels to form tributary networks (Bouma et al. 1991). Mudflow lobes develop at downslope termini of gullies where sediment flowing through a feature with negative relief (gully) coalesces to form a depositional feature with positive relief (Fig. 2; Coleman et al. 1980; Bentley et al. 2015). Lobes have an average thickness of 10 m, and coalesce and stack in a compensational manner analogous to sub-delta lobes and crevasse-splay deposits (Coleman et al. 1980).

Hurricane impact

Hurricanes are important triggers of mass movements offshore of the Mississippi River delta. The associated long-period/high-amplitude waves contribute to cyclic loading and unloading of the seabed, inducing bottom shear stresses capable of causing failure (Coleman et al. 1978). Guidroz (2009) studied historical hurricane impacts on the MRDF seabed in detail, and ascertained that only category 3+ hurricanes that slowly traverse the MRDF are likely to produce seabed mass failures of scales sufficient to induce catastrophic oil-platform collapse. Since the onset of Gulf of Mexico petroleum production, hurricanes in this category passing through or near MRDF include Betsy (in 1965), Camille (in 1969), Ivan (in 2004), and Katrina (in 2005). Mass movements associated with Hurricane Ivan destroyed seven platforms, and movements associated with Hurricane Katrina destroyed 46 platforms, with additional damage caused to infrastructure by both storms (Guidroz 2009).

Although catastrophic movements only occur during major hurricanes, weaker hurricanes, tropical storms, and winter cold fronts are capable of producing smaller seabed disturbances in shallower waters. Allison et al. (2005) observed a 20 cm deposit associated with tropical storm Isidore and Hurricane Lili in 2002. In a similar inner-shelf depositional environment on the southwest Louisiana coast, Denomme et al. (2016) observed bottleneck slides and collapse depressions in sidescan sonar data from water as shallow as 4 m; their rheological modeling suggests that waves associated with the passage of ~weekly winter cold fronts can generate failures in these water depths.

Changes in the modern Mississippi River

As part of the broader Mississippi River source-to-sink sedimentary system (Bentley et al. 2015), the modern Balize delta lobe of the MR is being strongly influenced by upstream anthropogenic alterations such as dams, diversions, and bank

stabilization that have reduced sediment load in the river's main stem. Additional factors influencing the delta land area and morphodynamics include local subsidence and eustatic sea-level rise (driving decreased sediment transport efficiency that accelerates in-channel sedimentation in the lower river), and upstream migration of major river discharge points (Kemp et al. 2014; Bentley et al. 2015). Allison et al. (2012) have shown that three outlets upstream of the Head of Passes (Fort St. Philip, Grand Pass, and Baptiste Collette) each currently discharge more suspended sediment than either South Pass or Pass a'Loutre (the two main distributary outlets other than SW Pass). Collectively, these phenomena are likely to lead to backstepping of the Balize delta lobe (Bentley et al. 2015). Blum and Roberts (2009, 2012) present a long-term decrease in the sediment load reaching the Gulf of Mexico, with as much as a 50% decline in the last century. One outcome may be an overall decrease and subsequent redistribution of sediment to different parts of the delta and continental shelf. This may increase the possibility of failures in historically stable areas fed by distributaries that are capturing more sediment, or reduce the driving forces for mass failures in areas where failures are presently driven in part by rapid sediment accumulation.

Sediment deposits and radionuclides on the continental shelf

Various sediment-dispersal processes may impart patterns in grain size, fabric, and radionuclide distributions that may be collectively diagnostic of those processes. Regarding hypopycnal plume delivery, Sommerfield and Nittrouer (1999) demonstrated that marine scavenging of $^{210}\text{Pb}_{\text{xs}}$ by fine sediment in river plumes may deplete marine $^{210}\text{Pb}_{\text{xs}}$ activity, producing zones of fine grain size (typical of plumes) and low $^{210}\text{Pb}_{\text{xs}}$ activity in sediment cores. When freshly deposited, these zones may also carry relatively high ^7Be activities and inventories, owing to the concentration of ^7Be in river catchments, and delivery to the coastal ocean by plume sediment (Sommerfield et al. 1999; Rotondo and Bentley 2003).

The study of radionuclides was applied on the Louisiana continental shelf during the 2000s to investigate regional dispersal and tropical cyclone deposits. Corbett et al. (2004) connected ^7Be inventories on the continental shelf with riverine-sourced sediment, because activities were greater than would be expected from fallout alone. They demonstrated that ^7Be and ^{137}Cs activities show transport of sediment across the shelf. Sediment transport away from the delta helps to explain the difference between measured sediment deposition rates (SDRs) of up to 4 cm/month (Corbett et al. 2004, ^7Be) and sediment accumulation rates (SARs) of up to 4 cm/year (Corbett et al. 2006, $^{210}\text{Pb}_{\text{xs}}$). As the ^7Be -laden sediments are transported away from the delta by wind-driven waves associated with fall and winter storms, ^{234}Th activity increases

with respect to ^7Be (Corbett et al. 2007). Concerning mass-movement events, Corbett et al. (2006) recognized slide deposits in chirp data; however, they did not attribute any patterns evident in radiochemical profiles to the influence of mass transport. Walsh et al. (2006) collected cores after the passage of hurricanes Katrina and Rita over the MRDF. All but one core had stratified deposits at the surface (indicative of suspension settling), while one core had mottled sediments with inclusions of larger clasts (indicative of a mudflow). Goni et al. (2007) showed that these deposits fined upward. $^{210}\text{Pb}_{\text{xs}}$ activity appears homogenized within both types of deposits, consistent with profiles measured by Allison et al. (2005) in event deposits associated with tropical cyclones Isidore and Lili.

Storm resuspension tends to produce beds (tempestites) that fine upward from erosional bases (e.g., Keen et al. 2012). Such beds may contain stair-step patterns in ^{210}Pb (and other radionuclide) activities wherein horizontal “treads” of the steps correspond to erosional bed contacts, and “risers” with relatively uniform activity tend to correspond to the deposited bed (Bentley et al. 2000, 2002; Keen et al. 2004); within these beds, additional variation in ^{210}Pb activity is commonly associated with variations in grain size, wherein sands have lower ^{210}Pb activity than muds. Sediment-gravity flows (both gravity-driven and those enhanced by waves and currents) may produce patterns in ^{210}Pb profiles similar to “stair-step” ^{210}Pb profiles in tempestites (Bentley and Nittrouer 2003; Rotondo 2004; Mullenbach and Nittrouer 2006; Muhammad et al. 2008).

Materials and methods

Field work and core processing

Cores were collected offshore of SW Pass between June 27th and July 3rd in 2014, from the R/V *Coastal Profiler* of the Louisiana State University’s Coastal Studies Institute. Cores were collected from four different facies (Fig. 2, Table 1) using an Ocean Instruments MC-400 multi-corer (<50 cm depth, 10 cm diameter) and a gravity corer with lead weights (up to 3 m depth, 10 cm diameter). Core locations are shown in Fig. 1b, c. Throughout the text, gravity cores are indicated by a “g” following the core location code. Depositional environments and facies were identified by the study of multi-beam bathymetry, sidescan, and subbottom seismic data collected from the R/V *Coastal Profiler* 1 week prior to coring (J. Obelcz et al., unpubl. data). Coring sites were selected to coincide either with subbottom seismic lines or with locations previously cored by Young (2014), who used analytical methods similar to those of this study, but over a wider area with lower sampling density. Maximum water depths for

coring were determined by the operational range of the swath sonar used by J. Obelcz et al. (unpubl. data) to map the seabed.

Of the four multi-core tubes collected per deployment, one was extruded on deck into 2 cm sections for radiochemical and grain size analysis, one was subsampled for X-radiography by inserting a two-piece tray (2 cm thick) with sliding lid to recover undisturbed stratigraphy and sedimentary structures, and two were subsampled with thin-walled plastic tubes (7.5 cm diameter) to archive undisturbed sediments for future study.

Gravity cores were analyzed on a Geotek MSCL-S® multi-sensor core logger for measurements of gamma density, magnetic susceptibility, and p-wave speed (of which only density is discussed here). Cores were subsequently split and sampled for grain size analysis, radiochemistry, and X-radiography (by extracting and archiving axial slabs 1.5 cm thick in clear acrylic plastic trays). All cores and subsamples were stored at 4 °C in a cold room until analysis.

Grain size analysis

Sediment was subsampled from the multi-core replicate that was extruded on deck or from the working half of the gravity cores after they were split. Small samples of wet sediment (<1 ml) were placed into test tubes with 40 ml of a 0.05% sodium metaphosphate solution to facilitate disaggregation, then dispersed in an ultrasonic bath (Hülse and Bentley 2012). No acid or hydrogen peroxide was used to remove carbonate or organic matter. Grain sizes were measured using a Beckmann-Coulter laser diffraction particle size analyzer (model LS 13 320). Data were then placed in volume-frequency contour plots generated using Sigmaplot® to graphically show the percent abundance of all grain sizes between 0.38 and 2,000 microns.

X-Radiography

Sediments preserved in acrylic trays from multi-core deployments as well as slabs preserved in trays after gravity cores were split were used to generate X-radiograph images. X-radiographs were taken using a Thales Flashscan 35 digital X-ray detector illuminated by a Medison Acoma portable X-ray unit operating at 4.8–5.4 mA and 60 keV. A total of 48 images were collected as 14-bit grayscale TIFF files and refined for observation using Adobe Photoshop.

Radionuclide analysis

Radionuclides of interest are ^7Be (natural cosmogenic, $t_{1/2}=53.2$ days), ^{210}Pb (natural ^{238}U series, $t_{1/2}=22.2$ years), and ^{137}Cs (anthropogenic fallout, $t_{1/2}=30.1$ years). Data are reported in decays per minute per gram dry sediment (dpm/g), for which 1 dpm=60 Bq. Water content was determined

Table 1 Summary of radionuclide data of multi-core samples. Averages were calculated without the values marked with an asterisk due to the poor fit to the data. Reported uncertainties reflect error propagation from the fit of Eq. 1 to radiochemical profiles. Abbreviations: *und* undisturbed, *gul* mudflow gully, *lob* mudflow lobe, *pro* prodelta

Station	Distance from SW Pass (km)	Facies	⁷ Be inventory (dpm/cm ²)	⁷ Be penetration depth (cm±1)	⁷ Be SDR (mm/day)	r ²	Age of deposit (days)	²¹⁰ Pb SAR (cm/year)	r ²
14-1	6.9	und	13.24	6	0.66±0.09	0.98	90.9±12.4	2.1±0.3	0.79
14-2	8.6	gul	10.76	6	0.96±0.55	0.78	62.5±35.8	2.8±1.2*	0.21*
14-3	10.4	lob	11.77	8	0.68±0.44	0.63	117.6±76.1	2.3±0.4	0.59
14-4	11.6	lob	4.08	6	0.86±0.06	0.97	69.8±4.5	2.9±0.3	0.79
14-5	5.27	gul	34.06	16	1.50±0.19	0.92	106.7±13.5	40.7±7.3*	0.01*
14-6	7.26	gul	6.57	6	0.33±0.04	0.99	181.8±21.5	2.8±0.5	0.61
14-7	9.38	und	2.85	4				1.5±0.1	0.86
14-8	11.54	lob	2.73	4				1.7±0.3	0.58
14-9	13.32	pro	6.26	6	0.62±0.3	0.84	96.8±46.8	2.4±0.4	0.62
14-10	11.6	und	4.51	4				2.4±0.3	0.79
14-11	10.9	lob	5.96	6	0.25±0.01	0.99	240.0±8.6	2.7±1.0*	0.32*
14-12	6.7	gul	15.73	10	0.50±0.05	0.99	200.0±19.2	1.3±0.2	0.68
14-15	8.8	gul	2.30	2				1.6±0.3	0.61
14-16	9.4	gul/lob	5.47	8	1.30±1.5*	0.37*	61.5±71.0*	3.7±1.2*	0.32*
14-18	9.2	gul	3.88	2				2.5±0.8*	0.35*
14-19	12.4	lob	3.45	4				5.3±4.5*	0.06*
Average			8.35	6.13	0.59±0.19	0.90	129.6±26.5	2.4±0.3	0.63

gravimetrically in samples for radionuclide analysis. Dried samples were then ground using a mortar and pestle, and sealed into petri dishes. Samples for ⁷Be measurement were analyzed within ~one half-life from the date of core collection. Samples for ²¹⁰Pb analysis rested in sealed dishes for 14 days before ²¹⁰Pb data were collected, to allow ingrowth of ²¹⁰Pb parent radionuclide ²²²Rn and to determine supported activities.

All samples were analyzed on Canberra LEGe 3825 or BEGe 3825 detectors calibrated for energy and efficiency using standard reference materials (US National Institute of Standards and Technology, and International Atomic Energy Agency), with samples from a single core being restricted to one detector. Detector efficiency for the 477 keV peak of ⁷Be (not present in the standards of this article) was determined by interpolation from adjacent peaks in NIST and IAEA standard reference materials. Sample self-absorption for ²¹⁰Pb gamma emissions was determined using the transmission method (Cochran and Masqué 2003). Activities associated with the 295 and 352 keV peaks of ²¹⁴Pb and the 609 keV peak of ²¹⁴Bi were averaged to determine the amount of supported ²¹⁰Pb. Supported ²¹⁰Pb activity is subtracted from total ²¹⁰Pb activity to determine excess ²¹⁰Pb (²¹⁰Pb_{xs}) activity.

Inventories of ⁷Be (decays per minute per square cm, dpm/cm²) were calculated by Eq. 1 from Muhammad et al. (2008):

$$I = \sum \rho_s \Delta z (1 - \Phi_i) A_i \quad (1)$$

where ρ_s is mineral density, Δz is thickness (cm) of the sample

in core i (2 cm), Φ_i is porosity (calculated by water loss at 60 °C), and A_i is ⁷Be activity (dpm/g). Long-term sediment accumulation rates (SARs) for ²¹⁰Pb and short-term sediment deposition rates (SDRs) for ⁷Be were calculated using Sigmaplot© by least-squares regressions on radionuclide data based on Eq. 2 from Muhammad et al. (2008) adapted from Nittrouer and Sternberg (1981):

$$A_z = A_0 e^{(-\lambda z / S)} \quad (2)$$

where A_z is activity at depth z (dpm/g), A_0 is activity extrapolated to the sediment surface (dpm/g), λ is the decay constant of radionuclide of interest (year⁻¹), and S is the sediment accumulation (long term, ²¹⁰Pb) or deposition (short term, ⁷Be) rate (cm/year, mm/day). The age of the ⁷Be-laden deposit was calculated by dividing the thickness of the ⁷Be-laden sediment by the deposition rates obtained by Eq. 2.

Results

Grain size

Frequency contour plots of grain size are shown in Fig. 3. Grain size does not vary greatly in the analyzed samples. Silt is the dominant grain size, making up 41–70% by volume. Most samples have a modal grain size in the very fine or fine silt range (6–8 Φ , 3.9–15.6 μ m). Clay content ranges from 16

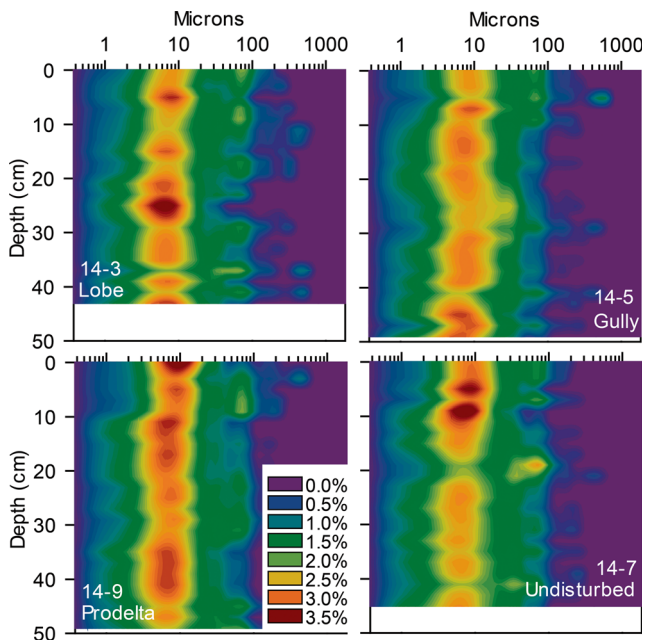


Fig. 3 Selected grain-size frequency plots representing depositional environments. All four cores have a modal grain size in the very fine/fine silt range (warm colors), as well as a few layers slightly enriched in very fine/fine sand. Colors in legend correspond to percent occurrence. See Fig. 1 for core locations

to 42%, and sand content from 0 to 39%. Thick sandy layers are not common; however, there is one 8 cm interval (36–44 cm depth) in gravity core 14-3g with 32–38% sand.

Gamma density

Figure 4 displays gamma-density profiles for gravity cores 14-3g (depositional lobe), 14-6g (mudflow gully), and 14-9g (prodelta). The density profiles do not show strong variations among the cores, or with depth within a single core. Much of the top section of core 14-3g (0–140 cm) varies slightly between values of 1.56 and 1.75 g/cm³, with a local maximum at 42 cm of 2.19 g/cm³. The lowest value of this core is 1.4 g/cm³ at a depth of 66 cm, and it does not correspond with deviations in any other measured data. The bottom section (140–292 cm) varies between 1.66 and 1.81 g/cm³, generally increasing down to a depth of 240 cm.

In core 14-6g, density increases to 1.66 g/cm³ at a depth of 60 cm, before decreasing to 1.37 g/cm³ at 68 cm, below which density varies little to the core base at 220 cm. The surface density of core 14-9g is 1.52 g/cm³. Density varies irregularly between 1.40 and 1.70 g/cm³ for the top 60 cm, before stabilizing to the bottom at 244 cm.

X-Radiography

X-radiographic images of cores reveal the sediments to be characterized by beds of cm to dm thickness, separated by

horizontal contacts with very low density contrast evident across contacts (Fig. 5a; 14-9g, prodelta). Not all bedding contacts are horizontal, as some appear convoluted (Fig. 5c; 14-6g, gully). Within-bed image shading indicative of graded bedding is not apparent. Vertical and inclined burrows <1 cm in diameter that appear to be open, or filled with very high-porosity sediment, are present but generally isolated and not ubiquitous (Fig. 5b; 14-19, lobe). Bioturbation is overall characterized by ichnofabric indices of 1–3 (i.e., approximately 0–20% of original bedding has been bioturbated; Droser and Bottjer 1986).

Radionuclide analysis

Results from ⁷Be analysis are shown in Figs. 6, 7 and 8. Generally, ⁷Be inventories (2.73–35.1 dpm/cm²), recent mass accumulation (1.2–8.7 g/cm²), and penetration depths (2–16 cm) decrease away from the river mouth. The apparent time since deposition for ⁷Be-laden sediment in each core was calculated from the deposit thickness and SDR, and ranged between 62.5 and 240 days, with an average age of 129.6 days. Results from all cores are displayed in Table 1. Sediment deposition rates ranged from 0.1 to 1.5 mm/day, with an average of 0.7 mm/day.

Beryllium activity is coincident with a muddy sediment drape slightly higher in porosity that is detectable in all cores (Fig. 7). There is no apparent relation between ⁷Be mass accumulation, penetration depth, or inventory compared to facies (undisturbed, gully, mudflow lobe, and prodelta); these

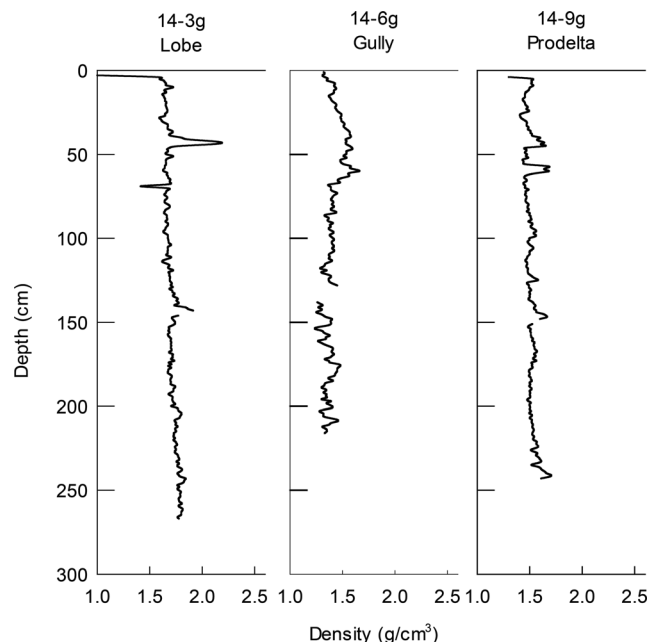


Fig. 4 Downcore density profiles for the gravity cores. Core 14-6g has a low density layer beginning at 68 cm depth, corresponding with a layer of homogenized ²¹⁰Pb_{xs} activity. Density variation decreases in the lower half of all three cores. See Fig. 1 for core locations

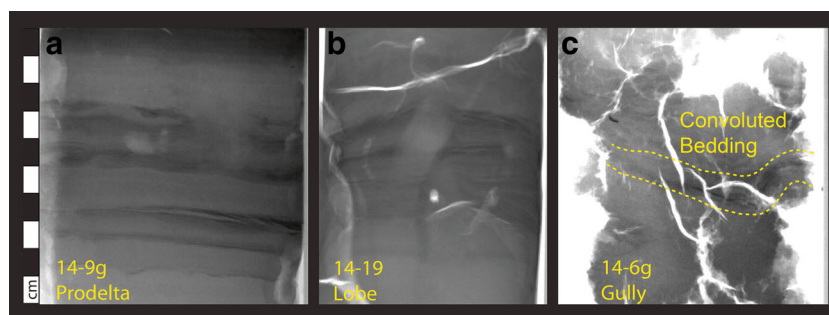


Fig. 5 Selected X-radiographs showing dominant sedimentary bedding features. **a** Thin horizontal bedding from core 14-9g (50–60 cm). **b** Bioturbated beds from core 14-19 (18–28 cm). **c** Convoluted bedding

from core 14-6g (185–195 cm). *White regions* Cracks and gaps produced during sampling and dewatering of very soft sediment. See Fig. 1 for core locations

measured values all decrease with increasing distance from SW Pass (Table 1, Figs. 6, 7 and 8).

Excess lead-210 ($^{210}\text{Pb}_{\text{xs}}$) activity declines gradually downcore from highest activities at the sediment surface (Figs. 9, 10 and 11), with undulatory subsurface maxima and minima to the base of multi-cores, and in all gravity cores except for 14-6g. Surface activity (0–6 cm) generally ranges between 4 and 12 dpm/g with the lowest values occurring at sites closest to SW Pass (Figs. 1, 8 and 9). The majority of the low-activity intervals do not correspond with obvious variations in clay content (clay-sized particles scavenge ^{210}Pb most effectively; Cochran and Masqué 2003). This trait is apparent in core 14-9, in the case of a low-activity interval at 22–32 cm depth for which there is no prominent grain size difference compared with sediments above or below (Figs. 3 and 9, lower left panel in each). One exception to this observation is shown in Fig. 10, where a low-activity zone in gravity core 14-3g coincides with the highest measured sand content in this study.

Apparent sediment-accumulation rates calculated from Eq. 2 range from 1.3 to 2.9 cm/year measured using $^{210}\text{Pb}_{\text{xs}}$ activity in ten multi-cores. Six values were rejected due to an r^2 value of less than 0.5. On average, accepted SARs calculated using $^{210}\text{Pb}_{\text{xs}}$ activity from multi-cores are 4.7 times lower than rates calculated using ^7Be (Table 1).

SARs calculated with $^{210}\text{Pb}_{\text{xs}}$ activity from gravity cores are noticeably greater than rates from the multi-cores (Table 2). Cores 14-3g, 14-6g, and 14-9g have rates of 6.0 cm/year (0–292 cm depth), 3.9 cm/year (0–70 cm) and 7.9 cm/year (0–246 cm) respectively. Activity generally decreases with depth for the entirety of core 14-3g, which is from a depositional lobe (Fig. 11). A pattern of alternating higher- and lower-activity intervals is superimposed on this trend. In gully core 14-6g, a general downward decrease of activity also occurs in the top 70 cm. Alternating intervals of high and low activity in core 14-6g are less pronounced than in 14-3g. Below 70 cm in core 14-6g, ^{210}Pb activity displays a nearly vertical trend with some variability to the bottom of the core (220 cm; Fig. 11). Activity decreases with depth in core 14-9g,

with indications of subsurface maxima and minima (50–150 cm) and a possible change in gradient below 200 cm (SAR for the 200–242 cm interval=2.2 cm/year, $r^2=0.90$); however, lower sampling density than for other cores does not allow for more detailed analysis (Fig. 11).

Cesium-137 was detected in every sample from multi-cores and gravity cores that underwent radionuclide analysis, to the base of each core. No prominent subsurface maxima (used as a time marker for the 1963 ^{137}Cs maximum environmental release; Robbins and Edgington 1975) were observed in any ^{137}Cs profiles. The presence of ^{137}Cs at the core bottom depth of 292 cm in core 14-3g indicates a sediment accumulation rate of >4.87 cm/year since ca. 1954 (Robbins and Edgington 1975), which is consistent with rates calculated using $^{210}\text{Pb}_{\text{xs}}$. The presence of ^{137}Cs in all samples also suggests all sediments in these cores were deposited since ca. 1954, and that deep penetration of excess ^{210}Pb into the seabed is not an artifact from inaccurate determination of supported ^{210}Pb activities.

Discussion

Based on previous studies of shelf sedimentary processes on the Mississippi River delta, dominant sediment dispersal processes in the present study area include suspension settling from hypopycnal river plumes (Moore and Scruton 1957; Coleman et al. 1980; Wright and Nittrouer 1995, and many others), storm wave/current-induced resuspension (Keen et al. 2006; Walsh et al. 2006; Xu et al. 2015), sediment slides and seabed flows driven primarily by gravity acting on a slope (Coleman et al. 1980; Denommee and Bentley 2013, and many others), and wave-current-enhanced sediment-gravity flows (Wright et al. 2001; Denommee et al. 2016). These criteria can serve to identify specific depositional and dispersal processes active during the time period encompassed by the core geochronologies of the present study. Horizontal bedding (Fig. 5a), which is consistent with suspension settling, is present at the surface of every core. While most of the collected

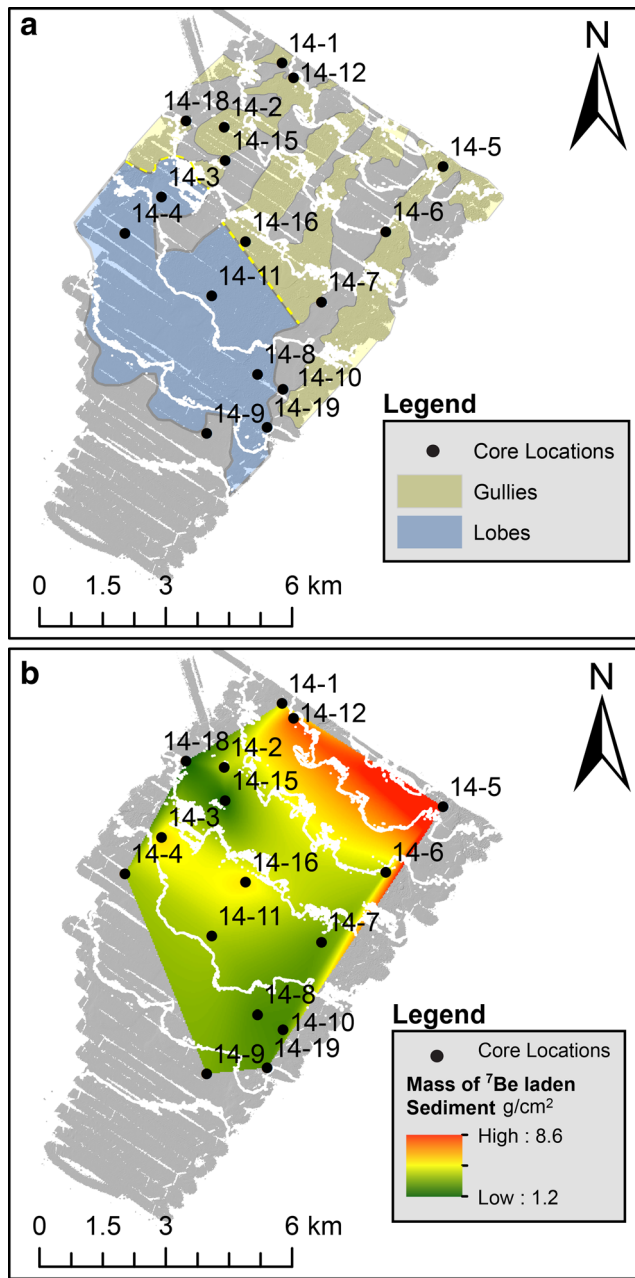


Fig. 6 **a** Facies distributions and core locations on contoured, hill-shaded bathymetry derived from Walsh et al. (2006), adapted from Fig. 1c. The yellow dashed line separating gully and lobe facies indicates a gradational boundary. Gray areas encompass undisturbed and prodelta facies, both of which are unaffected by mass movements. **b** Interpolated color-contoured map showing mass accumulation of sediment deposited in the 129 ±26 days calculated via ⁷Be activity. Results from each coring site were interpolated across the field area using the Natural Neighbor Interpolation method. The highest values occur in the northeast side of the field area, closest to SW Pass

material was deposited in horizontal beds, core 14-6g does contain some convolute laminations (Fig. 5c), which is consistent with rapid deposition and subsequent pore-fluid escape from buried sediment.

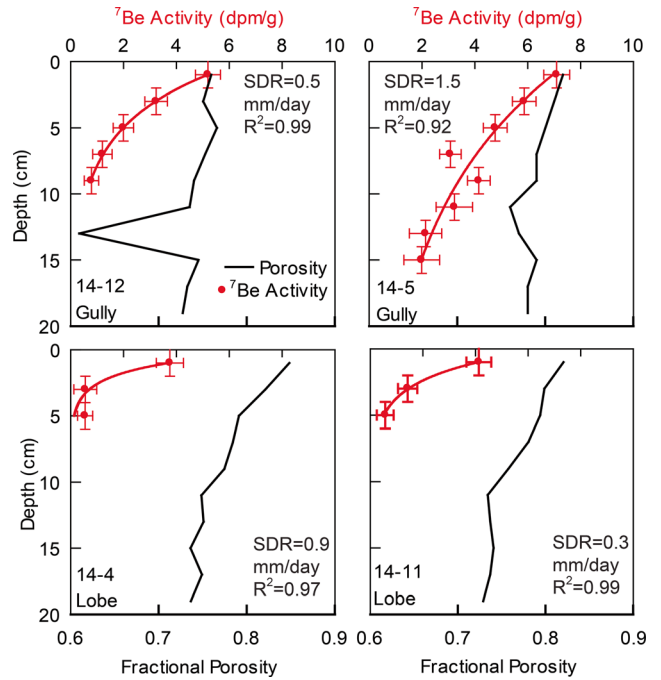


Fig. 7 Selected ⁷Be activity profiles and modeled sediment deposition rates. Cores 14-5 and 14-12 were taken from the northeastern-most part of the field area, closest to SW pass, and display the greatest depth of ⁷Be penetration. Cores 14-4 and 14-11 were taken farther from SW Pass, and display less ⁷Be penetration. Depositional facies of each core is indicated in the bottom left corner of each profile. See Fig. 1 for core locations

Sediment deposition rates for ⁷Be varied between 0.3–1.5 mm/day during peak flow conditions. The results of Allison et al. (2012) show up to a six-fold increase in daily sediment transport during the annual flood season (April to July). The highest measured water discharges during 2014 occurred during the 3 months prior to core collection (July; USACE 2015), indicating the greatest SDRs should occur

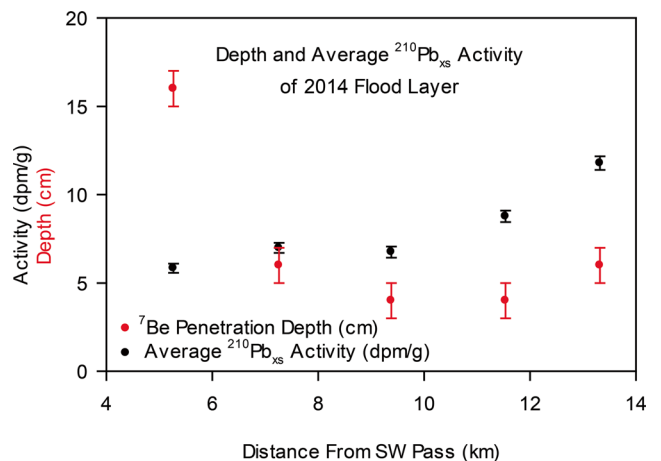


Fig. 8 Averaged ²¹⁰Pb_{xs} activity associated with the 2014 flood layer as detected along the transect from cores 14-5 to 14-9. Red circles Depth of ⁷Be penetration, which decreases in cores farther from SW Pass. Black circles Average ²¹⁰Pb_{xs} activity of samples for which ⁷Be was present. Average activity increases with distance from SW Pass, indicating increased lead scavenging from seawater

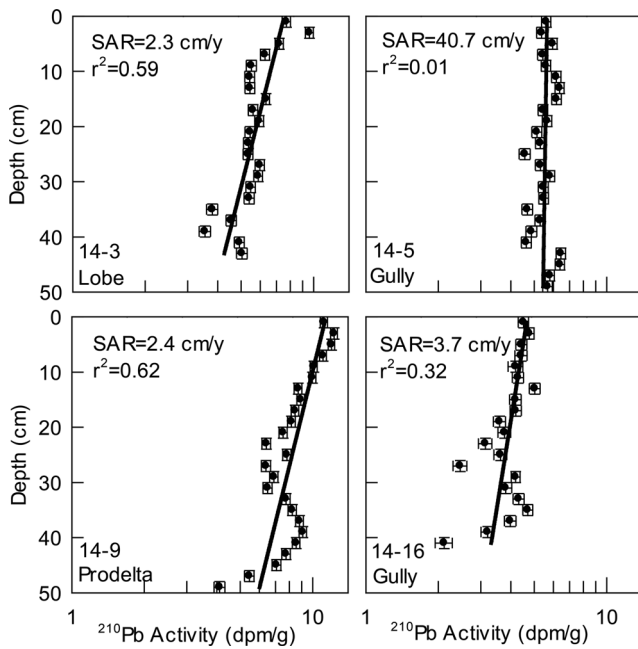


Fig. 9 Selected ^{210}Pb activity profiles exemplifying the varied nature of surface activity as well as the presence and absence of mid-core minima. See Fig. 1 for core locations

between April and June, and SDRs associated with low-flow seasons are likely much lower. The age of 129 ± 26 days for the ^7Be -laden sediment layer in multi-cores covers the span of the spring flood in 2014. The SDR obtained from ^7Be data can be used to form an upper estimate of annual sedimentation. When the average SDR of 0.7 mm/day is applied to the 4-month flood season, and a value 1/6 of the calculated SDR (derived from suspended sediment measurements presented in Allison et al. 2012) is applied to the rest of the year, the resulting annual sedimentation is 11.3 cm. This should be considered an upper estimate, given that 2 cm subsampling does not precisely measure ^7Be penetration depth. Even given

Fig. 10 Grain size (left) and $^{210}\text{Pb}_{\text{xs}}$ activity (right) in the top 50 cm of gravity core 14-3g. There are two layers of decreased $^{210}\text{Pb}_{\text{xs}}$ activity, one between 8–10 cm and another between 36–44 cm. The former does not correlate with a change in grain size, whereas the latter correlates with the highest sand content measured in any sample from this study

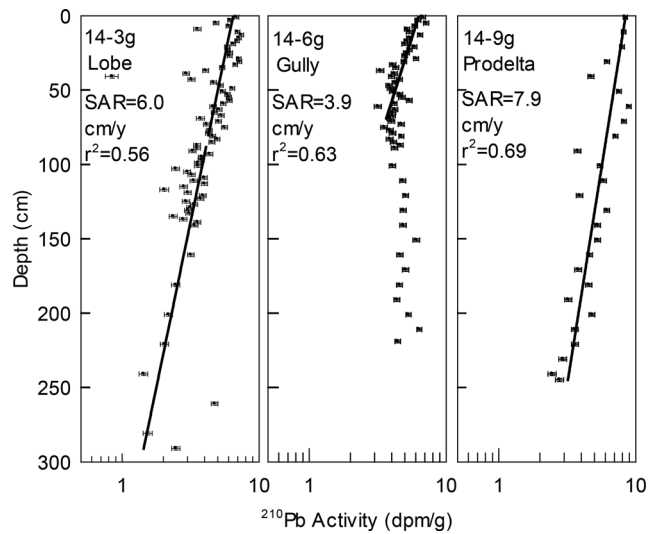
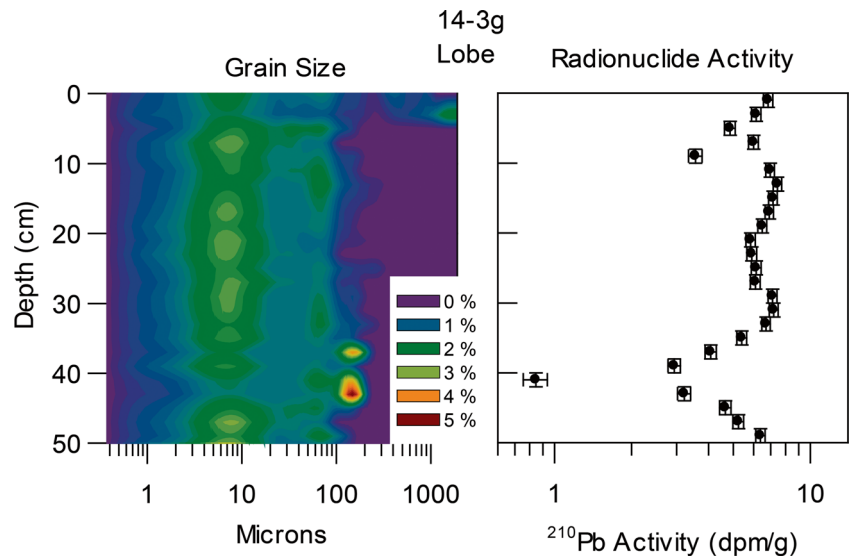


Fig. 11 ^{210}Pb profiles for gravity cores 14-3g (lobe), 14-6g (gully), and 14-9g (prodelta). Activity steadily declines for the entirety of 14-3g and 14-9g. Activity decreases for the top 70 cm of 14-6g, and remains constant for the bottom 150 cm of the core

the young age of the collected sediment cores, it is still possible to discern patterns of sediment deposition and retention.

Neither SARs nor SDRs appear to vary by facies (Table 1). Instead, radioisotope depositional patterns appear to vary as functions of distance from SW Pass, with higher depositional rates and ^7Be inventories and activities closer to SW Pass, and higher ^{210}Pb activities and lower SARs farther from SW Pass (Tables 1, 2; Figs. 6, 7, 8 and 11). Downcore variations of ^{210}Pb activities are mostly (but not always) independent of grain size (Fig. 10), suggesting that dissolved ^{210}Pb limitation, not grain size, controls sediment ^{210}Pb activities.

Sommerfield and Nittrouer (1999) demonstrated that rapidly deposited sediment on the continental shelf from the large 1995 flood on the Eel River retained the signal of a terrestrial source (low $^{210}\text{Pb}_{\text{xs}}$ activity). Initial flood pulses efficiently

Table 2 Comparison between gravity core and multi-core SAR. Abbreviations: *gul* mudflow gully, *lob* mudflow lobe, *pro* prodelta

Core	Facies	^{210}Pb SAR (cm/year)	r^2
14-3	lob	2.3±0.4	0.59
14-3g	lob	6.0±0.7	0.56
14-6	gul	2.8±0.5	0.61
14-6g	gul	3.9±0.5	0.63
14-9	pro	2.4±0.4	0.62
14-9g	pro	7.9±1.1	0.69

scavenged dissolved ^{210}Pb in the coastal zone, reducing the availability of marine-sourced dissolved ^{210}Pb for subsequent scavenging. Depletion of available marine-sourced ^{210}Pb can explain the activities associated with the 2014 flood deposit in the present study. Figure 8 shows the penetration depth of ^7Be (which marks sediment associated with the 2014 spring flood), as well as the ^{210}Pb activity associated with those intervals. $^{210}\text{Pb}_{\text{xs}}$ activity increases in the distal cores as the freshwater plume dispersed and scavenged more lead from the marine waters. Annual variations in the freshwater flux associated with spring flooding events should therefore drive variations in ^{210}Pb activity, which would be preserved in the sedimentary record. Furthermore, it is suggested that the undulatory nature of $^{210}\text{Pb}_{\text{xs}}$ profiles is not due to changes in grain size, as fine silt is the dominant grain in the majority of samples (Fig. 3).

Observations from the literature, the lack of erosional bases in X-radiographs, and the undulations in ^{210}Pb activity indicate that suspension settling from hypopycnal plumes of proximal river source (Wright and Nittrouer 1995; Sommerfield and Nittrouer 1999; Sommerfield et al. 1999) is the dominant dispersal process over the timeframe, sediment depth, and region encompassed by all multi-cores, and two gravity cores. Furthermore, sediment-gravity flows do not appear to be a major dispersal process over the same timeframe, sediment depth, and region. This timeframe includes a period of no major tropical cyclones since Hurricane Katrina (in 2005). The annual input of sediment from the MR is distributed across the field area with proximal sites receiving more than distal sites, regardless of the seafloor facies (which are controlled primarily by distribution of mass failures, not suspension settling from the plume).

The gravity cores provide a much longer record of activity, yielding long-term sediment-accumulation rates. Sediment-accumulation rates calculated from gravity cores where a regression (Eq. 2) could be properly fitted to the data are generally in agreement with average sedimentation rates from ^7Be in the multi-cores. The convergence of long-term $^{210}\text{Pb}_{\text{xs}}$ accumulation rates from gravity cores with short-term ^7Be rates confirms that much of the deposited sediment is not removed through resuspension or gravity-driven flow during the

timeframe captured in these cores. The preservation of multiple $^{210}\text{Pb}_{\text{xs}}$ -depleted flood deposits stacked along a decreasing trend line demonstrates a lack of sediment mixing via mass failure. It is suggested that the multi-cores return average sedimentation rates that are $2.5\times$ lower than the gravity cores because in the top ~ 50 cm of the seabed, the undulatory signature of the low-activity flood deposits provides more activity variation than does $^{210}\text{Pb}_{\text{xs}}$ radioactive decay over the same time period (Table 2). Activity profiles of $^{210}\text{Pb}_{\text{xs}}$ from gravity cores indicate that sediment-accumulation rates do not vary greatly with facies over longer scales than were captured in the multi-cores, with one exception detailed below.

Coleman et al. (1980) describe rapid and episodic progradation of mudflow lobes when the corresponding gully system is active, followed by a lack of progradation coupled with deposition of a cm- to dm-scale sediment cap that settled out of river plumes. These observations were based on repeated seafloor surveys using sidescan and subbottom sonar (Coleman et al. 1980). A sediment accumulation rate of 6.0 cm/year was calculated (cf. $^{210}\text{Pb}_{\text{xs}}$) using samples from 0–292 cm from mudflow lobe core 14-3g, which is in agreement with average sediment-accumulation rates across the area using ^7Be . This suggests that local retention of recently deposited sediment at this locality is high, and it is likely that little sediment within the 292 cm of sediment sampled by this core was reworked by mass failures in the last ~ 49 years (encompassing hurricanes Betsy in 1965, Camille in 1969, Ivan in 2004, and Katrina in 2005). While this core does not appear to contain an obvious record of homogenized mud deposited by mass failure, the sediment record from the top of the mudflow lobe core is comprised of mud settling out of the river plume, which (according to the results of Coleman et al. 1980) caps acoustically transparent mudflow deposits.

In mudflow gully core 14-6g, SAR from $^{210}\text{Pb}_{\text{xs}}$ activity over the interval 0–70 cm is 3.9 cm/year, which also falls in the range of river-plume SDRs. Scavenging effects (undulations of $^{210}\text{Pb}_{\text{xs}}$ activity not associated with grain size variations) do appear in this upper section of the core, consistent with other cores in the area. From 70 cm depth to the bottom of the core at 246 cm, the r^2 of a regression of Eq. 2 is poor (Table 2), the ^{210}Pb trend is nearly vertical with respect to depth, and the calculated sediment accumulation rate rises to 19 cm/year. Regressions using Eq. 2 for ^{210}Pb become less reliable at such high accumulation rates, owing to the sensitivity of the equation to slight gradient changes in ^{210}Pb activity versus depth (Hirschberg and Schubel 1979). This regression result is unlikely to represent actual sediment-accumulation rate; the poor fit of the line indicates that the observed $^{210}\text{Pb}_{\text{xs}}$ profile is not explained by steady-state deposition. Although sample density in this core section is lower than for upper sections, the $^{210}\text{Pb}_{\text{xs}}$ gradient in this portion of the core is extremely steep, which is likely indicative of rapid deposition or physical reworking (Nittrouer et al. 1984;

Bentley et al. 2002). These sediments likely represent a mudflow that deposited or reworked at least 176 cm of sediment (from 70 to 246 cm depth in the core).

Prodelta core 14-9g was collected from beyond the extent of the mudflow gullies and depositional lobes; the sediment accumulation rate (7.9 cm/year) calculated using this whole core is in agreement with ^7Be rates (Fig. 11). Profiles of ^{210}Pb appear to be similar for the upper 50 cm of sediment in both gravity and multi-cores from this station (Figs. 9 and 11). Fluctuations in $^{210}\text{Pb}_{\text{xs}}$ activity likely caused by plume scavenging dynamics appear to diminish below ~150 cm depth, and the $^{210}\text{Pb}_{\text{xs}}$ gradient near the base of the core indicates SAR=2.2 cm/year, suggesting variability in either scavenging, sediment accumulation, or both at this location over time.

The only apparent evidence of mass failure is captured in core 14-6g (Fig. 11). The zone of relatively uniform $^{210}\text{Pb}_{\text{xs}}$ activity begins at a depth of 70 cm, which is coincident with a drop in density captured by the whole core logger. Coleman et al. (1980) describe the movement of blocks with intact stratigraphy as well as remolded sediments, which are acoustically transparent in sonar images. The data from this core suggest that it was collected from a region of the seafloor that was remolded. Using ^7Be and ^{210}Pb sediment accumulation rates for upper and lower bounds, the flow occurred between 9 and 18 years ago, a period during which seven tropical cyclones passed within 100 km of the field area, including Ivan (in 2004) and Katrina (in 2005). A similar deposit of remolded sediment with homogenized $^{210}\text{Pb}_{\text{xs}}$ activity at a similar depth is absent in core 14-3g (Fig. 11), which was collected from a mudflow lobe sourced from a different mudflow gully. The lack of recent mass failures corresponds with a lull in tropical cyclone activity over the delta in the last 7 years (2006–2013) coupled with rapid sedimentation rates from the Mississippi River plume. These results suggest that strong seafloor shear stresses associated with major hurricanes are likely needed to drive mass failures on the upper delta front (10–70 m). However, bottleneck slides and collapse depressions were observed by Denommee et al. (2016) in much shallower waters (<10 m) triggered by strong cold front passages on the Atchafalaya shelf, underscoring the importance of mass-wasting events in sediment redistribution along muddy continental shelves.

Time-series bathymetric data (J. Obelcz et al., unpubl. data) from gully and lobe stations 14-6 and 14-3 respectively suggest that gully locations have deepened and lobes have shoaled each by 3 ± 0.5 m, despite no obvious core evidence for sediment-gravity flows at these locations during this timeframe. These contrasting results could be explained by the presence of a detachment surface below the depth sampled by gravity and multi-cores (0.5–3 m), above which sediments may be transported downgradient as a relatively cohesive and undisturbed block, consistent with previously observed “plug flow”

phenomena (Coleman et al. 1978), and below which deep-seated motions likely occur. This interpretation assumes that the block in motion has not rotated substantially, which is supported by generally horizontal subbottom reflectors (J. Obelcz et al., unpubl. data). However, if block rotation did occur, then this interpretation of deep radioisotope profiles could be invalidated. Because the present study is focused mainly on the top 0.5 or 3 m of cores on the seabed, the possibility of subsurface mass failure with a detachment surface deeper than 3 m cannot be excluded during the last ~7 years.

Conclusions

This study provides insights on the geochronology of the upper delta front of the Mississippi River, in particular the signals of recent deposition and mass failure. Analysis of sediment cores from four depositional facies provided a multifaceted approach to the study of mass-wasting events and accumulation patterns. The major findings can be summarized as follows:

1. Beryllium-7 activity shows that 2–16 cm of sediment was delivered to the study area by the MR during the spring flood of 2014, prior to core collection. Sedimentation rates are highest near the SW Pass distributary, diminish with distance offshore, and do not correlate to morphological facies.
2. $^{210}\text{Pb}_{\text{xs}}$ activities associated with the 2014 flood are variable and increase with distance from SW Pass. There are several intervals of decreased $^{210}\text{Pb}_{\text{xs}}$ activity that do not correlate with changes in clay content. These data suggest that the amount of lead scavenging varies annually and spatially in the field area as a hypopycnal plume disperses seaward.
3. $^{210}\text{Pb}_{\text{xs}}$ SARs from the longer gravity cores (avg. 5.9 cm/year) converge with ^7Be SDRs, indicating that, in the absence of catastrophic sediment mass-transport events in the top 3 m of seabed induced by major hurricanes, most of the annually deposited sediment is retained on the delta front. Any weaker transport events that have occurred have not left diagnostic mass-transport signatures.
4. Mass failures can be detected by their physical properties preserved in sediment cores. A layer of homogenized $^{210}\text{Pb}_{\text{xs}}$ activity corresponding with a layer of low density from a mudflow gully gravity core is indicative of a mass-failure deposit. There was no such layer recorded in the gravity core from a mudflow lobe, but other studies (Coleman et al. 1980) note that older flows were covered by river-plume deposits with internal stratigraphy.

Acknowledgements This study was funded by the Department of Interior Bureau of Ocean Energy Management, under the cooperative agreement M13AC00013, via the Louisiana State University Coastal Marine Institute program. We would like to thank the field support group of the Coastal Studies Institute of Louisiana State University for their invaluable help during field operations, as well as all others who assisted. We are grateful to all of the undergraduate students who performed laboratory analyses. Also acknowledged are Jeffrey Obelcz for helpful input, two reviewers for constructive assessments of an earlier version of this article, as well as the journal editors.

Compliance with ethical standards

Conflict of interest The authors declare that there is no conflict of interest with third parties.

References

- Allison MA, Sheremet A, Goni MA, Stone GW (2005) Storm layer deposition on the Mississippi-Atchafalaya subaqueous delta generated by Hurricane Lili in 2002. *Cont Shelf Res* 25:2213–2232. doi:10.1016/j.csr.2005.08.023
- Allison MA, Demas CR, Ebersole BA, Kleiss BA, Little CD, Meselhe EA, Powell NJ, Pratt TC, Vosburg BM (2012) A water and sediment budget for the lower Mississippi–Atchafalaya River in flood years 2008–2010: implications for sediment discharge to the oceans and coastal restoration in Louisiana. *J Hydrol* 432–433:84–97. doi:10.1016/j.jhydrol.2012.02.020
- Bea RG (1971) How sea floor slides affect offshore structures. *Oil Gas J* 69:88–92
- Bentley SJ Sr (2002) Dispersal of fine sediments from river to shelf: process and product. *Gulf Coast Assoc Geol Soc Trans* 52:1055–1067
- Bentley SJ, Nittrouer CA (2003) Emplacement, modification, and preservation of event strata on a flood-dominated continental shelf: Eel shelf, Northern California. *Cont Shelf Res* 23:1465–1493. doi:10.1016/j.csr.2003.08.005
- Bentley SJ, Furukawa Y, Vaughan WC (2000) Record of event sedimentation in Mississippi Sound. *Gulf Coast Assoc Geol Soc Trans* 50: 715–723
- Bentley SJ, Keen TR, Blain CA, Vaughan WC (2002) The origin and preservation of a major hurricane event bed in the northern Gulf of Mexico: Hurricane Camille, 1969. *Mar Geol* 186:423–446. doi:10.1016/S0025-3227(02)00297-9
- Bentley SJ Sr, Blum MD, Maloney J, Pond L, Paulsell R (2015) The Mississippi River source-to-sink system: perspectives on tectonic, climatic, and anthropogenic influences, Miocene to Anthropocene. *Earth-Sci Rev* 153:139–174. doi:10.1016/j.earscirev.2015.11.001
- Blum MD, Roberts HH (2009) Drowning of the Mississippi Delta due to insufficient sediment supply and global sea-level rise. *Nat Geosci* 2: 488–491. doi:10.1038/ngeo553
- Blum MD, Roberts HH (2012) The Mississippi Delta region: past, present, and future. *Annu Rev Earth Planet Sci* 40:655–683
- Bouma AH, Roberts HH, Coleman JM, Prior DB (1991) Delta-front gullies as part of mass-movement phenomena; Mississippi River delta front. *Special Publication SEPM* 46:99–105
- Cochran JK, Masqué P (2003) Short-lived U/Th series radionuclides in the ocean: tracers for scavenging rates, export fluxes and particle dynamics. *Rev Mineral Geochem* 52:461–492. doi:10.2113/0520461
- Coleman JM, Prior DB, Garrison LE (1978) Submarine landslides in the Mississippi River Delta. *Proc Offshore Technology Conf* 10. doi:10.4043/3170-MS
- Coleman JM, Prior DB, Garrison LE (1980) Subaqueous sediment instabilities in the offshore Mississippi River delta. *Open File Report* 80-02. US Department of the Interior, Bureau of Land Management
- Corbett DR, McKee B, Duncan D (2004) An evaluation of mobile mud dynamics in the Mississippi River deltaic region. *Mar Geol* 209:91–112. doi:10.1016/j.margeo.2004.05.028
- Corbett DR, McKee B, Allison MA (2006) Nature of decadal-scale sediment accumulation on the western shelf of the Mississippi River delta. *Cont Shelf Res* 26:2125–2140. doi:10.1016/j.csr.2006.07.012
- Corbett DR, Dail M, McKee B (2007) High-frequency time-series of the dynamic sedimentation processes on the western shelf of the Mississippi River delta. *Cont Shelf Res* 27:1600–1615. doi:10.1016/j.csr.2007.01.025
- Denommee K, Bentley S (2013) Influence of mass-transport processes on clinoform mechanics on the southwest Louisiana Shelf. *Gulf Coast Assoc Geol Soc Trans* 63:205–212
- Denommee K, Bentley SJ Sr, Harazim D, Macquaker JHS (2016) Hydrodynamic controls on sedimentary fabric development in a shelf clinothem: Southwest Louisiana Continental Shelf. *Mar Geol*. doi:10.1016/j.margeo.2016.09.013
- Droser ML, Bottjer DJ (1986) A semiquantitative field classification of ichnofabric: research method paper. *J Sed Res* 56:558–559
- Galloway WE (1975) Process framework for describing the morphologic and stratigraphic evolution of deltaic depositional systems. In: Broussard ML (ed) *Deltas: Models for exploration*. Houston Geologic Survey, Houston, TX, pp 87–98
- Goni MA, Alleau Y, Corbett DR, Walsh JP, Mallinson D, Allison MA, Gordon E, Petsch S, Dallapenna TM (2007) The effects of Hurricanes Katrina and Rita on the seabed of the Louisiana shelf. *Sed Record* 5:4–9
- Guidroz WS (2009) Subaqueous, hurricane-initiated shelf failure morphodynamics along the Mississippi River Delta Front, North-Central Gulf of Mexico. *Dissertation*, Louisiana State University and A&M
- Hart BS, Hamilton TS, Barrie JV (1998) Sedimentation rates and patterns on a deep-water delta (Fraser Delta, Canada): integration of high-resolution seismic stratigraphy, core lithofacies, and ¹³⁷Cs fallout stratigraphy. *J Sediment Res* 68:556–568
- Hirschberg DJ, Schubel JR (1979) Recent geochemical history of flood deposits in the northern Chesapeake Bay. *Estuar Coastajourl Mar Sci* 9:771–777. doi:10.1016/S0302-3524(79)80010-9
- Hooper JR, Suhayda JN (2005) Hurricane Ivan as a geologic force: Mississippi Delta Front seafloor failures. *Proc Offshore Technology Conf Paper* no 17737. doi:10.4043/17737-MS
- Hülse P, Bentley SJ (2012) A ²¹⁰Pb sediment budget and granulometric record of sediment fluxes in a subarctic deltaic system: the Great Whale River, Canada. *Estuar Coast Shelf Sci* 109:41–52. doi:10.1016/j.ecss.2012.05.019
- Kaiser MJ, Yu Y, Jablonowski CJ (2009) Modeling lost production from destroyed platforms in the 2004–2005 Gulf of Mexico hurricane seasons. *Energy* 34:1156–1171
- Keen TR, Bentley SJ, Chad Vaughan W, Blain CA (2004) The generation and preservation of multiple hurricane beds in the northern Gulf of Mexico. *Mar Geol* 210:79–105. doi:10.1016/j.margeo.2004.05.022
- Keen T, Furukawa Y, Bentley S, Slingerland R, Teague W, Dykes J, Rowley C (2006) Geological and oceanographic perspectives on event bed formation during Hurricane Katrina. *Geophys Res Lett* 33, L23614. doi:10.1029/2006GL027981
- Keen TR, Slingerland RL, Bentley SJ Sr, Furukawa Y, Teague WJ, Dykes J (2012) Sediment transport on continental shelves: storm bed formation and preservation in heterogeneous sediments. *Int Assoc Sedimentol Spec Publ* 44:295–310
- Kemp GP, Willson CS, Rogers JD, Westphal KA, Binsalam SA (2014) Adapting to change in the lowermost Mississippi River: implications for navigation, flood control and restoration of the delta

- ecosystem. In: Perspectives on the Restoration of the Mississippi Delta. Springer, Heidelberg, pp 51–84
- Lee HJ, Greene HG, Edwards BD, Fisher MA, Normark WR (2009) Submarine landslides of the Southern California Borderland. Special Paper Geol Soc Am 454:251–269. doi:10.1130/2009.2454(4.3)
- Meade RH (1996) River-sediment inputs to major deltas. In: Coastal Systems and Continental Margins, vol 2: Sea-level rise and coastal subsidence. Kluwer, Dordrecht, pp 63–85
- Moore DG, Scruton PC (1957) Minor internal structures of some recent unconsolidated sediments. AAPG Bull 41:2723–2751
- Muhammad Z, Bentley SJ, Febo LA, Droxler AW, Dickens GR, Peterson LC, Opydyke BN (2008) Excess ^{210}Pb inventories and fluxes along the continental slope and basins of the Gulf of Papua. J Geophys Res Earth Surf 113:F01S17. doi:10.1029/2006JF000676
- Mullenbach B, Nittrouer C (2006) Decadal record of sediment export to the deep sea via Eel Canyon. Cont Shelf Res 26:2157–2177
- Nittrouer C, Sternberg R (1981) The formation of sedimentary strata in an allochthonous shelf environment: the Washington continental shelf. Mar Geol 42:201–232
- Nittrouer CA, DeMaster DJ, McKee BA, Cutshall NH, Larsen IL (1984) The effect of sediment mixing on Pb-210 accumulation rates for the Washington continental shelf. Mar Geol 54:201–221. doi:10.1016/0025-3227(84)90038-0
- Prior DB, Coleman JM (1982) Active slides and flows in underconsolidated marine sediments on the slopes of the Mississippi Delta. In: NATO Conference Series, vol 6: Marine slides and other mass movements, vol 6. Plenum, New York, pp 21–49
- Prior DB, Suhayda JN (1979) Submarine mudslide morphology and development mechanisms, Mississippi Delta. Proc Offshore Technol Conf 11:1055–1061. doi:10.4043/3482-MS
- Prior D, Suhayda JN, Lu NZ, Bornhold BD, Keller GH, Wiseman WJ, Wright LD, Yang ZS (1989) Storm wave reactivation of a submarine landslide. Nature 341:47–50
- Robbins JA, Edgington DN (1975) Determination of recent sedimentation rates in Lake Michigan using Pb-210 and Cs-137. Geochim Cosmochim Acta 39:285–304
- Rotondo K (2004) Transport and deposition of fluid mud event layers along the Western Louisiana Inner Shelf. Thesis, Louisiana State University and A&M
- Rotondo KA, Bentley SJ (2003) Deposition and resuspension of fluid mud on the western Louisiana inner shelf. Gulf Coast Assoc Geol Soc Trans 53:722–731
- Shepard FP (1955) Delta-front valleys bordering the Mississippi distributaries. Geol Soc Am Bull 66:1489–1498. doi:10.1130/0016-7606(1955)66[1489:Dvbtmd]2.0.Co;2
- Slingerland R, Driscoll NW, Milliman JD, Miller SR, Johnstone EA (2008) Anatomy and growth of a Holocene clinothem in the Gulf of Papua. J Geophys Res Earth Surf 113:F01S13. doi:10.1029/2006JF000628
- Sommerfield CK, Nittrouer CA (1999) Modern accumulation rates and a sediment budget for the Eel shelf: a flood-dominated depositional environment. Mar Geol 154:227–241
- Sommerfield CK, Nittrouer CA, Alexander CR (1999) ^{7}Be as a tracer of flood sedimentation on the northern California continental margin. Cont Shelf Res 19:335–361. doi:10.1016/S0278-4343(98)00090-9
- Sterling GH, Strohbeck EE (1973) The failure of the South Pass 70 “B” Platform Hurricane Camille. Proc Offshore Technol Conf 27:263–268. doi:10.4043/1898-MS
- Sultan N, Voisset M, Marsset B, Marsset T, Cauquil E, Colliat J-L (2007) Potential role of compressional structures in generating submarine slope failures in the Niger Delta. Mar Geol 237:169–190. doi:10.1016/j.margeo.2006.11.002
- USACE (2015) Miss River Discharge Hydrograph. United States Army Corp of Engineers. <http://rivergages.mvr.usace.army.mil/WaterControl/Districts/MVN/tar.gif>. Accessed 13 Nov 2015
- Walsh JP, Nittrouer CA (2009) Understanding fine-grained river-sediment dispersal on continental margins. Mar Geol 263:34–45. doi:10.1016/j.margeo.2009.03.016
- Walsh JP, Corbett DR, Mallinson D, Goni M, Dail M, Lowey K, Marcinak K, Ryan K, Smith C, Stevens A, Summers B, Tesh T (2006) Mississippi Delta mudflow activity and 2005 Gulf Hurricanes. EOS Trans Am Geophys Union 87:477–478
- Wright L, Coleman JM (1973) Variations in morphology of major river deltas as functions of ocean wave and river discharge regimes. AAPG Bull 57:370–398
- Wright LD, Nittrouer CA (1995) Dispersal of river sediments in coastal seas - 6 Contrasting cases. Estuaries 18:494–508. doi:10.2307/1352367
- Wright L, Friedrichs C, Kim S, Scully M (2001) Effects of ambient currents and waves on gravity-driven sediment transport on continental shelves. Mar Geol 175:25–45
- Xu K, Harris CK, Hetland RD, Kaihatu JM (2011) Dispersal of Mississippi and Atchafalaya sediment on the Texas-Louisiana shelf: model estimates for the year 1993. Cont Shelf Res 31:1558–1575. doi:10.1016/j.csr.2011.05.008
- Xu K, Mickey RC, Chen Q, Harris CK, Hetland RD, Hu K, Wang J (2015) Shelf sediment transport during hurricanes Katrina and Rita. Comput Geosci 90:24–39. doi:10.1016/j.cageo.2015.10.009
- Young DR (2014) Examination of the 2011 Mississippi River flood deposit on the Louisiana continental shelf. Thesis, East Carolina University